How to cite: *Angew. Chem. Int. Ed.* **2024**, *63*, e202401950
doi.org/10.1002/anie.202401950

Valence Tautomerism

Molecular Twist-Induced Single-Crystal Isomerization and Valence Tautomeric Transitions in a Cobalt-Dioxolene Complex

Ling-Tai Yue, Svetlana O. Shapovalova, Jie-Sheng Hu, Maxim G. Chegerev, Yu-Meng Zhao, Cheng-Dong Liu, Meng Yu, Alyona A. Starikova,* Alexander A. Guda, Zi-Shuo Yao, and Jun Tao**

Dedicated to Professor Osamu Sato of Kyushu University for his 60th birthday.

Abstract: A mononuclear valence tautomeric (VT) complex, $[Co(pycz)_2(Sq)(Cat)]$ (**1-*trans***), where pycz = 9-(pyridin-4-yl)-9*H*-carbazole, $Sq^{\bullet-}$ = 3,5-di-*tert*-butyl-semiquinonato, and Cat^{2-} = 3,5-di-*tert*-butyl-catecholato, is synthesized in the *trans* configuration, which undergoes one-step valence tautomeric transition above room temperature. Remarkably, **1-*trans*** can transform into its isomeric structure, $[Co(pycz)_2(Sq)(Sq)]$ (**1-*cis***), at temperature above 350 K in a single-crystal-to-single-crystal way by *in situ* molecular twist, and the resulting **1-*cis*** exhibits a pronounced two-step VT transition during magnetic measurements that is rare for mononuclear VT complexes. Such drastic solid-state structural transformation is reported in VT compounds for the first time, which is actuated by a crystal surface's melting-recrystallization induced phase transition process. DFT calculations offer an underlying mechanism suggesting a concerted bond rotation during the structural transformation. The results demonstrate an unconventional approach that realizes structural transformation of VT complexes and the control of VT performance.

[*] L.-T. Yue, J.-S. Hu, Y.-M. Zhao, C.-D. Liu, Prof. M. Yu, Prof. Z.-S. Yao, Prof. J. Tao
Key Laboratory of Cluster Science of Ministry of Education, School of Chemistry and Chemical Engineering
Beijing Institute of Technology
Liangxiang Campus, Beijing 102488 (China)
E-mail: mengyu@bit.edu.cn
taojun@bit.edu.cn

S. O. Shapovalova, Prof. A. A. Guda
The Smart Materials Research Institute
Southern Federal University
Sladkova 178/24, Rotov-on-Don 344090 (Russian Federation)

M. G. Chegerev, Prof. A. A. Starikova
Institute of Physical and Organic Chemistry
Southern Federal University
Stachka Avenue 194/2, Rotov-on-Don 344090 (Russian Federation)
E-mail: aastarikova@sfedu.ru

Introduction

Valence tautomeric (VT) complexes have gained significant attention due to their ability to enable reversible electron transfer between the redox-active ligand and metal center under external stimuli.[1] Particularly appealing are those demonstrate hysteretic bistability and/or multi-step spin-state switching that offer enhanced functionality and logic complexity.[2] In this context, the manipulation of VT properties through isomeric construction has emerged as a versatile approach, such as bidirectional *cis-trans* photoswitching of 4-styrylpyridine and photoisomerism of spirooxazine- and diarylethene-based ligands.[3] Nevertheless, while the isomerization transitions typically require photo-responsive groups and are usually only achievable in solution or amorphous state, the direct utilization of the isomerization in complex configurations seems to offer broader applicability. Only a few reports have highlighted solvent-triggered isomerism phenomena,[4] yet the presence of solvent molecules in the lattice hinders comprehensive comparison and elucidation of the structure–activity relationship. Hence, the exploration of melting-mediated, *in situ* single-crystal-to-single-crystal (SCSC) isomerization involving dynamic coordination bonds in VT complexes remains largely unexplored. This structural isomerization presents an ideal testbed, enabling a direct examination of the impacts of coordination environment, stacking modes, and intermolecular interactions on VT transitions, thus establishing a precise structural-property relationship to guide the design of VT complexes.

Here we show that a cobalt-dioxolene complex, $[Co(pycz)_2(Sq)(Cat)]\cdot 5CH_3OH\cdot CH_2Cl_2$ (**1-*trans*·*S***) [pycz = 9-(pyridin-4-yl)-9*H*-carbazole, $Sq^{\bullet-}$ = 3,5-di-*tert*-butyl-semiquinonato, Cat^{2-} = 3,5-di-*tert*-butyl-catecholato], and its desolvated form, **1-*trans***, undergo similar one-step gradual VT transitions with unexpected abnormality at high temperature. This abnormality is attributed to a thermal-activated molecular isomerization in the solid state from the *trans*(N)-*trans*(^{t}Bu) configuration to the *trans*(N)-*cis*(^{t}Bu) one (Scheme 1). Of particular interest is that the resulting complex, **1-*cis***, displays a two-step VT behavior that is unprecedented among mononuclear VT complexes. The elucidation of this unprecedented solid-state *trans*-to-*cis* isomerization contributes to the understanding of the under-

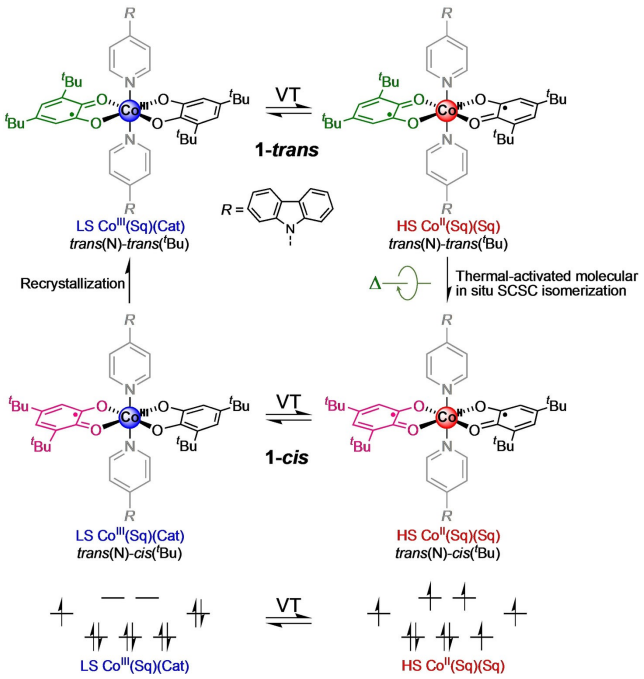

Scheme 1. Structural demonstration of electronic states and structural isomerization involved in this study.

lying mechanism and interactions governing VT behavior, and our research offers valuable insights for the rational design and synthesis of novel VT complexes with tailored properties.

Results and Discussion

Synthesis

The monodentate ligand pycz was synthesized via a nucleophilic substitution reaction involving 4-fluoropyridine hydrochloride and 9*H*-carbazole in the presence of NaH in DMF (Scheme S1, Supporting Information, SI). Subsequently, the cobalt-dioxolene complex **1-*trans*·*S*** was synthesized using the layer diffusion method in a glass tube, resulting in the formation of dark green crystals at room temperature (SI). Following this process, the desolvated form of **1-*trans*·*S***, denoted as **1-*trans***, was obtained by subjecting **1-*trans*·*S*** to an elevated temperature of 326 K in vacuum for 12 h, with thermogravimetric analysis (TGA) indicating the complete removal of solvent molecules at this temperature, while the complex is stable below 450 K (Figure S1). The isomeric complex, **1-*cis***, was obtained by heating **1-*trans*·*S*** or **1-*trans*** at an elevated temperature (365 K) under N_2 atmosphere for 6 h. Additionally, **1-*trans*** was also obtained by volatilizing a chloroform solution of **1-*cis***, as a meaningful attempt. The phase purity of all samples was confirmed by powder X-ray diffraction (PXRD) (Figure S2) and elemental analyses. Detailed synthetic procedures are provided in the Supporting Information.

Magnetic Properties

The $\chi_M T$ versus T plots of **1-*trans*·*S*** in the cooling and warming modes overlap perfectly below 300 K (Figure 1). The $\chi_M T$ value at 100 K is 0.62 $cm^3 mol^{-1} K$, which exceeds the spin-only value (0.375 $cm^3 mol^{-1} K$) expected for an electronic configuration of [LS-$Co^{III}(pycz)_2(Sq)(Cat)$] with $S = {}^1/_2$. This suggests the presence of residual HS-Co^{II} species resulting from an incomplete VT transition[5] and the temperature independent paramagnetism (TIP) of Co^{III}.[6] Upon temperature increasing, an upsurge from 350 K in $\chi_M T$ are observed attributed to VT transition accompanied by solvent loss.[7] At 378 K, an unexpected maximum of 3.52 $cm^3 mol^{-1} K$ is reached. Upon further warming, the $\chi_M T$ value declines gradually unexpectedly. The final $\chi_M T$ value of 3.38 $cm^3 mol^{-1} K$ at 390 K indicates a HS configuration of [HS-$Co^{II}(pycz)_2(Sq)(Sq)$] (2.6–4.5 $cm^3 mol^{-1} K$).[5c,8] Thus, we can conclude that a thermal-induced VT transition, LS-Co^{III}–$Sq^{\bullet-}$/Cat^{2-}→HS-Co^{II}–$Sq^{\bullet-}$/$Sq^{\bullet-}$, is observed in **1-*trans*·*S***. To compare, magnetic measurements were conducted on the desolvated complex, **1-*trans***. Below 340 K, **1-*trans*** exhibits a more gradual VT transition with a $\chi_M T$ value of 2.59 $cm^3 mol^{-1}$ K at 340 K. Surprisingly, upon further heating, the downward-upward characteristic is still observed, wherein the $\chi_M T$ value reaches a local maximum of 3.55 $cm^3 mol^{-1}$ K at 370 K, a minimum of 3.37 $cm^3 mol^{-1} K$ at 380 K, and then increases to 3.82 $cm^3 mol^{-1}$ K at 390 K, respectively (Figure 1). Further investigation attributes this unusual "reverse VT"-like phenomenon to a thermal-induced structural isomerization (i.e. **1-*trans*→1-*cis***, see below).

At the end of measuring **1-*trans*** (390 K), the subsequent $\chi_M T$ versus T curve (red) is not superimposable with the first cooling and heating cycle (blue) due to the formation of **1-*cis***, revealing a distinct two-step feature associated with VT

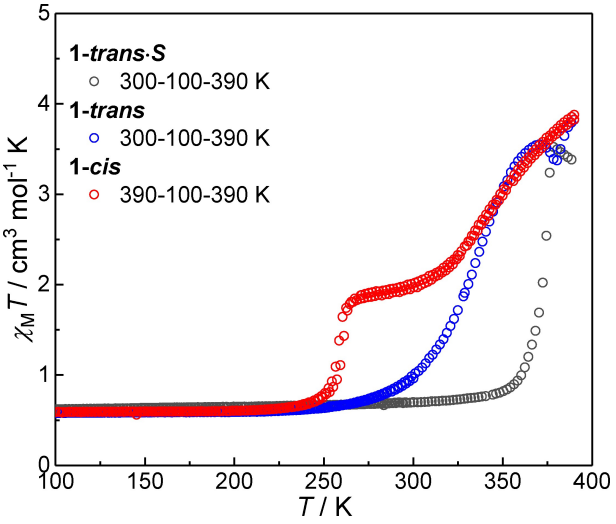

Figure 1. $\chi_M T$ versus T plots of **1-*trans*•*S*** (black circle) and **1-*trans*** (blue circle) in the thermal cycles of 300→100→390 K, and **1-*cis*** in the thermal cycle of 390→100→390 K. The measurement of **1-*cis*** begins at the end of measuring **1-*trans***. Temperature scan rate: 2 $K min^{-1}$, applied magnetic field: 5000 Oe.

transition (Figure 1). During the cooling process, $\chi_M T$ gradually decreases until it reaches an inclined plateau around 1.97–1.90 $cm^3 mol^{-1} K$ within the temperature range of 300–265 K, corresponding approximately to a 50 % VT conversion. Subsequently, a sharp decline in $\chi_M T$ occurs, resulting in a value of 0.75 $cm^3 mol^{-1} K$ at 250 K, which undergoes only a slight decrease to 0.59 $cm^3 mol^{-1} K$ at 100 K. The two-step VT transition is reproducible during the subsequent heating cycle, featuring a small hysteresis loop of 2 K-wide between 250 and 270 K. The two-step VT transition is confirmed through differential scanning calorimetric (DSC) measurements (Figure S3), which reveal two sets of endothermic and exothermic peaks that indicate the occurrence of two distinct thermal events. To the best of our knowledge, such pronounced two-step VT behavior represents the second example in mononuclear VT complexes,[9] as it typically requires dinuclear systems.[2b–e] It is worth mentioning that the two-step feature can be observed for either **1-*trans*·*S*** or **1-*trans*** during the second measuring cycle (Figure S4).

Crystal Structures

Single-crystal X-ray diffraction (SCXRD) analysis revealed that **1-*trans*·*S*** adopts the monoclinic space group $P2_1/n$ at 250 K (Table S1). The asymmetric unit contains a whole complex molecule, one disordered CH_2Cl_2 molecule, and five CH_3OH molecules. The cobalt ion is six-coordinated with four O atoms from two dioxolene ligands in the equatorial plane, and two axial pyridyl N atoms from two pycz ligands (Figure 2, left). The average bond lengths of Co–O (1.884 Å) and Co–N (1.945 Å) are characteristic of a LS-Co^{III} state. The C–O bond lengths lie on the borderline between the typically ranges for $Sq^{\bullet-}$ and Cat^{2-}, suggesting the presence of a mixed-valent character (Table S2). Thus, the electronic structure of **1-*trans*·*S*** at 250 K can be assigned as [LS-Co^{III}(pycz)$_2$(Sq)(Cat)]. The complex molecules are organized in one-dimensional (1D) chains along the *c*-axis through intermolecular stacking of adjacent pycz ligands, and two-dimensional (2D) supramolecular grids are constructed on the *ac* plane through extensive interchain C–H···π interactions involving the *tert*-butyl groups and carbazole rings. These 2D layers further stack along the *b*-axis direction, with solvent molecules located within the interlayer gaps (Figure S5). For comparison, SCXRD analysis was performed on **1-*trans***, which was prepared by subjecting the single crystal of **1-*trans*·*S*** to a temperature of 326 K for 12 hours. The space group of **1-*trans*** is $P2_1/c$ at 150 K, accompanied by a considerable reduction in the unit cell volume by 19.7 % (Table S1), and the asymmetric unit and bond metrics closely resemble those observed in **1-*trans*·*S*** at the [LS-Co^{III}(pycz)$_2$(Sq)(Cat)] electronic state (Table S2). Notably, the crystal packing effects lead to a variation in the dihedral angle between the axial pyridine rings, shifting from 0.2° to 33.5° (Figure 2a,b). Additionally, the dihedral angles between the pyridine and carbazole rings experience changes from 38.3°/38.7° to 32.7°/35.4°. The supramolecular architecture of **1-*trans*** follows a similar fashion to that of **1-*trans*·*S***. The most prominent alteration involves a decrease in the interlayer distance along the *b* axis due to the removal of solvent molecules (the shortest Co–Co distance between layers has changed from 11.812 Å to 10.109 Å), leading to a slight slip along the *b* axis and an overall more densely packed structure (Figures S5 and S6).

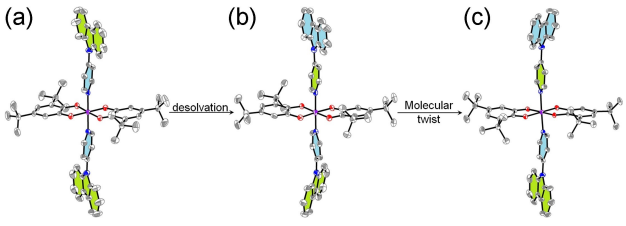

Figure 2. Perspective view of the molecular structures in **1-*trans*·*S*** (a), **1-*trans*** (b), and **1-*cis*** (c) with 50% thermal ellipsoids. Hydrogen atoms and solvent molecules are omitted for clarity. Approximate ring coplanarity of opposite pycz ligands is indicated by the same color filling. Atom color codes: gray, C; blue, N; purple, Co; red, O.

To gain insights into the structural factors underlying the anomalous magnetic behavior, *in situ* variable-temperature SCXRD analyses were performed on **1-*trans***. At 340 K, **1-*trans*** retains the $P2_1/c$ space group, but exhibits elongation in all unit cell axes, resulting in a 3.5 % increase in unit-cell volume compared to the structure at 150 K. Moreover, the Co–O and Co–N bond lengths are extended to an average value of 1.970 Å and 2.062 Å, respectively, while the dioxolene C–O bond lengths undergo a contraction from an average of 1.329 Å to 1.301 Å. These observations are consistent with a VT transition from [LS-Co^{III}(pycz)$_2$(Sq)(Cat)] to [HS-Co^{II}(pycz)$_2$(Sq)(Sq)]. However, bond valence sum (BVS) and MOS calculations (ligand oxidation state analysis by least-squares fitting of dioxolene C–C and C–O bond lengths, the catecholate and semiquinonate forms have MOS values of −2 and −1, respectively)[10] reveal that the VT conversion is incomplete (Table S2), which aligns with the magnetic data. Upon elevation of the temperature to 365 K, a space group transformation from $P2_1/c$ to $C2/c$ is observed, accompanied by a 180° rotation of one of the dioxolene groups. This conformational change gives rise to a distinct *cis*-oriented arrangement of the *tert*-butyl groups, resulting in the formation of the **1-*cis*** isomer that is stable in the whole temperature range in the solid state (Figure 2c). Notably, since Pierpont et al. reported the first example of cobalt dioxolene-based VT complex,[11] subsequent studies on similar systems have predominantly shown *trans*-oriented conformations. Hence, from a structural standpoint, the presence of this *cis*-oriented conformation is quite exceptional. Considering the extensive structural rearrangement associated with this *trans*-to-*cis* process, the ability of the transformation to occur in a densely packed solid state while maintaining crystallinity is both remarkable and perplexing. It is worth mentioning that **1-*cis*** can also be obtained in bulk by incubating **1-*trans*** at 365 K. Thus, it can be inferred that the observed anomalous magnetic behavior is attributed to the temperature-induced *in situ* formation of **1-*cis***.

Variable-temperature SCXRD analysis for **1-*cis*** was then conducted. At 365 K, the asymmetric unit contains a half-complex molecule, with Co–N and Co–O bond lengths featuring average values of 2.111 Å and 2.003 Å, respectively, and dioxolene C–O bonds having an average of 1.298 Å. These bond metrics, along with the results of bond valence sum (BVS) and MOS calculations (Table S2), suggest a further shift in the electronic configuration towards [HS-$Co^{II}(pycz)_2$(Sq)(Sq)]. Counterintuitively, the expansion of the coordination sphere around the cobalt center leads to a decrease in unit cell volume by 1.0 % compared to **1-*trans*** at 340 K (Table S1). This can be attributed to a contraction along the *b* axis (direction of molecular dipole moment), resulting from a more efficient interlayer packing between the 2D layers. Specifically, the *cis*- conformation in **1-*cis*** alleviates steric hindrance around the dioxolene oxygens from one side, making them more prone to hydrogen bonding with *tert*-butyl groups from adjacent layers. This arrangement results in a corrugated pattern along the *c*-axis direction, facilitating interlayer stacking (Figure 3). Furthermore, independent gradient model (IGM) analyses[12] (visual study of weak interaction) also demonstrate that the *cis*- conformation is more conducive to the formation of more weak interactions between the layers, effectively reducing their distance (Figure S7). Additionally, in **1-*cis***, the pycz ligands exhibit a tendency for stronger π···π stacking interactions along the *c* direction compared to **1-*trans***, as evidenced by multiple C–H···π interactions (Figure S7). At 270 K, a point in the middle of the $\chi_M T$ plateau, **1-*cis*** maintains the *C*2/*c* space group with shortened average Co–N and Co–O bond lengths (2.038 Å and 1.944 Å, respectively). However, the C–O bond lengths remain almost identical to those at 365 K. Traditionally, dioxolene C–O bond length is used as an indicator of ligand oxidation state. By this criterion, assigning the electronic state at 270 K to [LS-$Co^{II}(pycz)_2$(Sq)(Sq)] seems tempting.[9] However, this assignment can be readily ruled out by XAS spectroscopy (Figure S8), UV/Vis-NIR (Figure S9), IR (Figure S10), EPR (Figure S11) and DFT calculations (see below). Ligand oxidation state analyses together with BVS calculations also suggest the absence of a [LS-$Co^{II}(pycz)_2$-(Sq)(Sq)] intermediate state (Table S2). At 150 K, the Co–N/O and C–O bond lengths correspond to a [LS-$Co^{III}(pycz)_2$(Sq)(Cat)] electronic state, in agreement with the magnetic data. Notably, a change in space group to $P2_1/n$ is observed, resulting in significant structural changes in **1-*cis***. Besides slight differences in intermolecular interactions due to unit cell contraction, the most notable distinction is the alteration in the crystallographic packing pattern along the *c*-axis direction. Unlike the high-temperature phase (HP) at 365 K and intermediate-temperature phase (IP) at 270 K, where the carbazole units stack in a *"H*-aggregate*"* format, the low-temperature phase (LP) at 150 K undergoes reorganization to arrange in a *"H*-aggregate*"*-*"J*-aggregate*"*-*"H*-aggregate*"* repetitive fashion (Figure S12). This arises from the fact that the two carbazole units in each complex molecule engage in two different sets of π stacking interactions, with one set significantly stronger than the other, which is supported by IGM analysis (Figure S7).

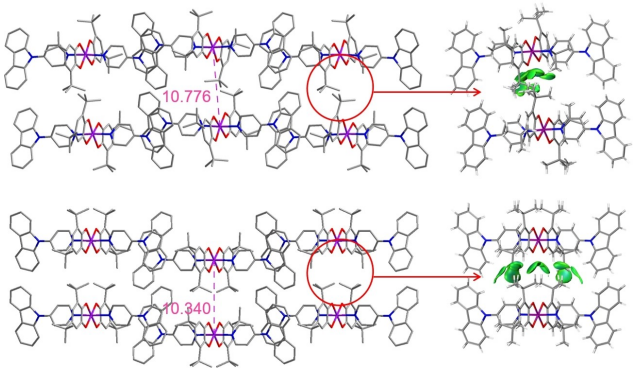

Figure 3. Crystal packings of **1-*trans*** (top) at 340 K and **1-*cis*** (down) at 365 K on the *bc* plane. **1-*cis*** adopts a corrugated pattern along the *c*-axis direction. The distance between layers (Co–Co) has decreased from 10.776 Å to 10.340 Å. The visualization of noncovalent interactions (IGM analyses) in **1-*trans*** and **1-*cis*** are also shown (right).

Isomerization Mechanism

Room-temperature PXRD patterns reveal that **1-*trans*** and **1-*cis*** exhibit prominent peaks at 10.40° and 10.85°, respectively (Figure S2), which correspond to the diffraction of the (0 2 0) plane aligning with the aforementioned 2D supramolecular plane (Figure 3). Variable-temperature PXRD experiments were conducted to shed light on the structural transformation from **1-*trans*** to **1-*cis***, by heating **1-*trans*** from 340 to 405 K (Figure 4a and S13). As a result, a major difference in the diffraction pattern was observed, with the peak slightly shifted to a higher angle at 10.85° for **1-*cis***. In addition, between 340 and 365 K, the diffraction peak exhibits a slight shift from 10.40° to 10.45°, with the intensity remaining almost unchanged. This can be attributed to VT transition of **1-*trans*** that dominates within this temperature range, resulting in an expansion of the cobalt coordination sphere and a simultaneous decrease in the distance between the (0 2 0) planes. As the temperature further increases, continuous decreases in peak intensity accompanied by a shift to higher angles are observed, indicating the gradual transformation of **1-*trans*** into **1-*cis*** that completes at 405 K. Interestingly, upon reversing the temperature back to 340 K, the PXRD pattern remained characteristic of **1-*cis*** (Figure S13), suggesting that the isomerization process is irreversible in the solid state.

To investigate the kinetics of the SCSC isomerization process, we conducted time-dependent *in situ* magnetic measurements for **1-*trans***. The $\chi_M T$ values of **1-*trans*** and **1-*cis*** exhibit a significant difference between 270 K and 280 K, providing a useful indicator for the ratio of **1-*trans*** and **1-*cis*** (Figure 1). The progress of isomerization at 365 K was tracked by monitoring the ratio of **1-*cis*** (α) over time, and the results presented in Table S3 and Figure S14. The obtained data clearly demonstrate that the transformation rate decelerates, as indicated by the curve shape commonly observed in diffusion-controlled reactions,[13] even with a

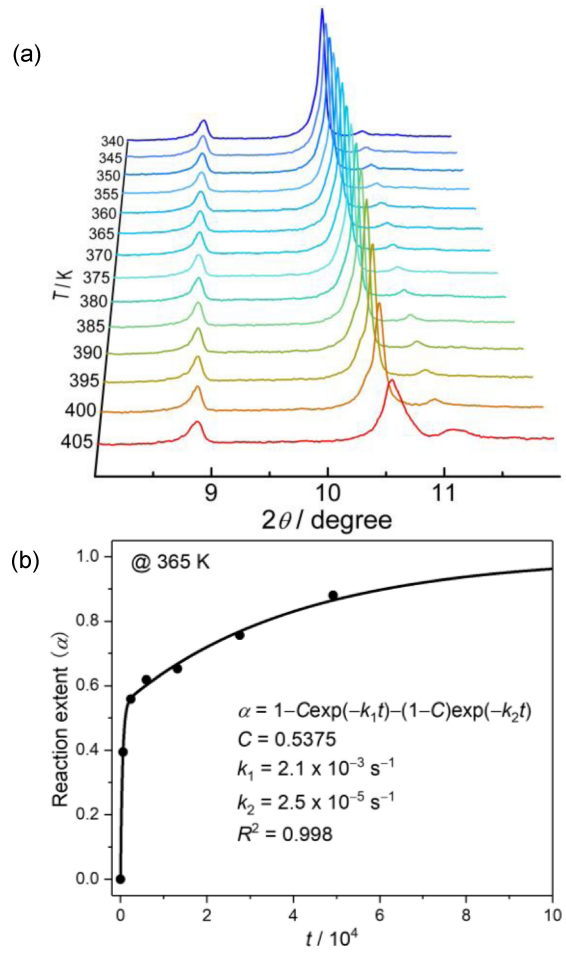

Figure 4. Overlay of variable-temperature PXRD patterns of **1-*trans*** (a), for clarity a perspective projection angle of 15 degree, an X-axis offset of 10, and a Y-axis offset of −76 are chosen for drawing. The isomerization kinetics for crystals of **1-*trans*** at 365 K (b). The black line represents the kinetic curve fitted to the expression.

limited number of available data points. Due to the complexity of the solid-state isomerization process, conventional formulas used for describing solid-state reaction kinetics are not suitable.[14] Instead, we employed an approximation relationship[15] to fit the obtained data, as given by equation (1):

$$\alpha = 1 - C\exp(-k_1 t) - (1 - C)\exp(-k_2 t) \quad (1)$$

The rate components k_1 and k_2 are $2.1\times10^{-3}\,s^{-1}$ and $2.5\times10^{-4}\,s^{-1}$, respectively, with $C = 0.5375$ (Figure 4b). The rapid composition corresponds to the nucleation and growth of crystal, possibly starting from the surface of the crystal or defects inside the crystal, while the slow composition might be linked to a process that involves annealing.[15]

DSC measurements of **1-*trans*** at various heating rates showed distinctive feature consisting of an initial endothermic peak rapidly followed by an exothermic peak (Figure S15a). Such a characteristic pattern is commonly associated with simultaneous crystal melting and recrystallization process.[16] The endothermic peak corresponds to the melting of **1-*trans*** and the isomerization reaction, while the subsequent exothermic peak can be attributed to the crystallization process of **1-*cis***. Indeed, the crystal surfaces exhibit randomly distributed nucleation spots upon heating, indicative of crystal melting and recrystallization (Figure S16 and Video S1).[15] The complexity of this process is influenced by the heating rate. At the lowest heating rate ($1.0\,°C\,min^{-1}$), the endothermic peak becomes barely discernible, analogous to the challenge of observing crystal melting. Conversely, when rapidly heating the crystals of **1-*trans*** ($50\,°C\,min^{-1}$) to 410 K, only a molten state was observed under a microscope (Figure S15b and S17). Thus, it is evident that heating not only induces the melting of **1-*trans*** by disrupting intermolecular interactions but also provides the necessary energy for the isomerization process. Because the occurrence of isomerization entailing significant structural reorganization is inconceivable in the solid state within such a densely packed environment, the associated energy penalty is simply insurmountable without any obvious energy compensation mechanism, as confirmed by DFT calculations (see below). Therefore, we propose that the presence of a molten state is of paramount significance for facilitating the isomerization process by providing an amorphous and flexible environment that lowers the energy cost.

The isomerization mechanism encompassing three main thermodynamic processes (Scheme 2): VT transition, crystal melting/recrystallization, and *trans*-to-*cis* isomerization. As temperature increases, **1-*trans*** gradually converts from the LS-Co^{III} state to the HS-Co^{II} state. When temperature exceeds 350 K, the intermolecular interactions of **1-*trans***-$(HS\text{-}Co^{II})_c$ begin to be disrupted, leading to crystal surface or defect area melting and the formation of **1-*trans***$(HS\text{-}Co^{II})_m$ molten phase (the subscripts *c* and *m* represent the crystalline and molten states, respectively). Simultaneously, *trans*-to-*cis* isomerization occurs, establishing a thermodynamic equilibrium between **1-*trans***$(HS\text{-}Co^{II})_m$ and **1-*cis***$(HS\text{-}Co^{II})_m$, which are essentially isoenergetic according to DFT calculations. However, the melting point of **1-*cis***$(HS\text{-}Co^{II})_m$ is likely higher than that of **1-*trans***$(HS\text{-}Co^{II})_m$, owing to its stronger intermolecular interactions (Figure S7) and more polar molecular conformation (0.5 D of **1-*cis***$(HS\text{-}Co^{II})$ vs 0 D of **1-*trans***$(HS\text{-}Co^{II})$, Figure S18). Drawing from our

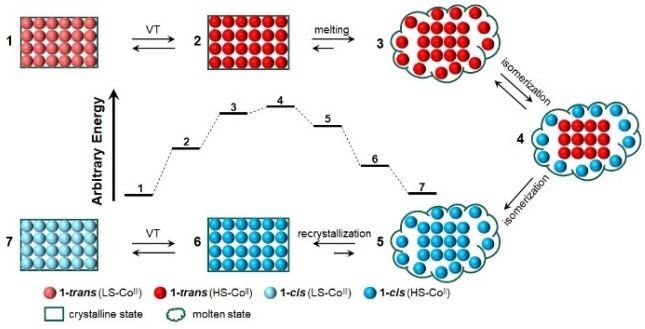

Scheme 2. Mechanistic illustration of VT transition and *trans*-to-*cis* isomerization.

observations and consistent with previously studied cases,[16a] the isomerization reaction tends to proceed from the low-melting isomer to that with a higher melting point. Calculated thermodynamic parameters from DSC measurements show the exothermic nature of the transformation process from **1-*trans***(HS-Co^{II})$_c$ to **1-*cis***(HS-Co^{II})$_c$ (Table S4, $|\Delta H_{END}| < |\Delta H_{EXO}|$), which demonstrates that the isomerization process is thermodynamically favored. Consequently, **1-*cis***(HS-Co^{II})$_m$ is prone to recrystallization, resulting in the formation of **1-*cis***(HS-Co^{II})$_c$. This leads to a decrease in the population of **1-*cis***(HS-Co^{II})$_m$, shifting the *trans*-to-*cis* equilibrium towards the **1-*cis***(HS-Co^{II})$_m$ side and driving the isomerization reaction forward until all **1-*trans*** species are consumed. The transformation process primarily involves melting-mediated isomerization of **1-*cis***, followed by recrystallization. Remarkably, the **1-*cis*** isomer possesses a more polar molecular conformation compared to **1-*trans*** isomer, as illustrated in Figure S18. This results in stronger intermolecular interactions, a more efficient mode of packing, enhanced lattice stabilization as shown in Figure 3 and S7, and ultimately a higher melting point and lower potential energy, as depicted in Figure S15a and Table S4. We contend that the driving force behind this isomerization is intricately linked to an increased interaction between molecules in the **1-*cis*** isomer, stemming from dipole-dipole interaction. According to literature, the decrease in cooperativity from solid to molten state, which arises from weakened intermolecular interactions, can lead to slower magnetic transition, as shown in Figure S19, i.e., a smaller $\chi_M T$ value at the same temperature.[17] Consequently, the "reverse-VT" phenomenon is synchronized with the isomerization during the melting from **1-*trans***(HS-Co^{II})$_c$ to **1-*cis***(LS-Co^{III})$_m$. Similarly, the small dip near 380 K can be attributed to the subsequent increase in cooperativity during the recrystallization from **1-*cis***(LS-Co^{III})$_m$ to **1-*cis***(HS-Co^{II})$_c$. Nonetheless, entropic factors associated with the phase transition and isomerization processes cannot be excluded.[18]

The isomerization reactions in metal chelates with tropolonate, catecholate, and dithiocarbamate ligands are mainly governed by non-bond-rupture twist mechanisms, as described by Bailar and Rây–Dutt twist. This is in contrast to acetylacetonate complexes, which commonly involve intramolecular bond-rupture mechanisms.[19] Experimental evidence often shows that bond rupture is indicated by high $\triangle H^{\neq}$ and positive $\triangle S^{\neq}$ values.[20] Kepert has established parameters for these relationships and defined the measurement of chelates based on the electrostatic model.[21] Accordingly, complexes with smaller bite *b* values ranging from 1.25 to 1.37 are more likely to experience non bond-rupture twist in isomerization (Table S5).[20,22] In our study, the kinetic data does not conform to a simple first-order reaction model, which has hindered the determination of the thermodynamic activation parameters related to the isomerization mechanism. Nevertheless, the normalized bites *b* values for **1-*trans***(HS-Co^{II})$_c$ and **1-*cis***(HS-Co^{II})$_c$ fall within the range favorable for twist mechanisms (1.32 and 1.30, respectively), as established by Kepert's findings.

DFT Calculations

To shed light on the electronic and magnetic properties of **1-*trans*** and **1-*cis*** and possible mechanism of *trans*-to-*cis* isomerization, DFT computational modeling was performed. The computed electronic energy differences for the HS-Co^{II}–$Sq^{\bullet-}$/$Sq^{\bullet-}$ and LS-Co^{III}–$Sq^{\bullet-}$/Cat^{2-} electromers are 6.4 kcal mol$^{<M->1}$ and 9.7 kcal mol$^{<M->1}$ for **1-*trans*** and **1-*cis***, respectively (Table S6). These values fall within the typical range for the VT transition of cobalt-dioxolene complexes,[23] indicating the potential occurrence of a thermally initiated LS-Co^{III}–$Sq^{\bullet-}$/Cat^{2-}⇌HS-Co^{II}–$Sq^{\bullet-}$/$Sq^{\bullet-}$ transition. Notably, Olshansky's recent report emphasized the significance of the LS-Co^{II}–$Sq^{\bullet-}$/$Sq^{\bullet-}$ intermediate state in driving a two-step VT transition.[9] However, our calculated results reveal that the LS-Co^{II}–$Sq^{\bullet-}$/$Sq^{\bullet-}$ electromer has a higher relative energy than the others, making it unlikely to be observed, as its formation from the closest energy electromer HS-Co^{II}–$Sq^{\bullet-}$/$Sq^{\bullet-}$ would require a decrease in system entropy with increasing temperature, which is improbable (Table S6, Figure S20–22).

The LS-Co^{III}–$Sq^{\bullet-}$/Cat^{2-} electronic states of **1-*trans*** and **1-*cis*** compounds are virtually isoenergetic. Surprisingly, a comparison of the HS-Co^{II}–$Sq^{\bullet-}$/$Sq^{\bullet-}$ electronic states between **1-*trans*** and **1-*cis*** reveals an energy preference for the former by 3.6 kcal mol^{-1} (Table S6), implying that the isomerization process is not primarily thermodynamically driven, at least not at the molecular level. Nevertheless, the insignificant energy difference suggests that the *cis*-configuration can still be populated at higher temperature, given a reasonable activation energy. To elucidate a probable mechanism for the *trans*-to-*cis* isomerization process, we started calculations with the model system **1-*trans'*** comprising two pyridine molecules instead of carbazole rings (Figure S23,24 and Table S7). Since the isomerization is observed at high temperature, at which **1-*trans*** exists mostly in the HS-Co^{II}–$Sq^{\bullet-}$/$Sq^{\bullet-}$ electronic state, all the calculations were performed on the sextet potential energy surfaces (PES). In the isomerization processoccurring via a concerted bond rotation without bond breakage, the energetics involving three transition states and two intermediates does not exceed 10 kcal mol^{-1} (Table S7, Figure S23), which allows us to expect its thermal accessibility.

We then recalculated the energy profile for the *trans*-to-*cis* isomerization based on the bond rotation mechanism using the real structure of **1-*trans*** (Figure 5, Table S8). The complex **1-*trans*** undergoes three consecutive Rây–Dutt twists, culminating in its transformation into **1-*cis***. Each rotation occurs around a pseudo C_3 axis of the complex, with the pseudo C_3 faces are O1O2N1, O1O3O4, and O3O4N1, respectively, generating a pseudo-C_{2v} symmetric transition state. Initially, **1-*trans*** converts into an intermediate structure, ***Int*1** ($\Delta E^{ZPE} = 2.0$ kcal mol^{-1}), characterized by a *cis*-orientation of the pycz ligands and an almost perpendicular arrangement of $Sq^{\bullet-}$ planes, via ***TS*1** with an energy barrier of 10.7 kcal mol^{-1}. It is noteworthy that this critical configuration has been previously observed experimentally in a VT complex,[4] which lends credence to our proposed mechanism. The subsequent structural rearrange-

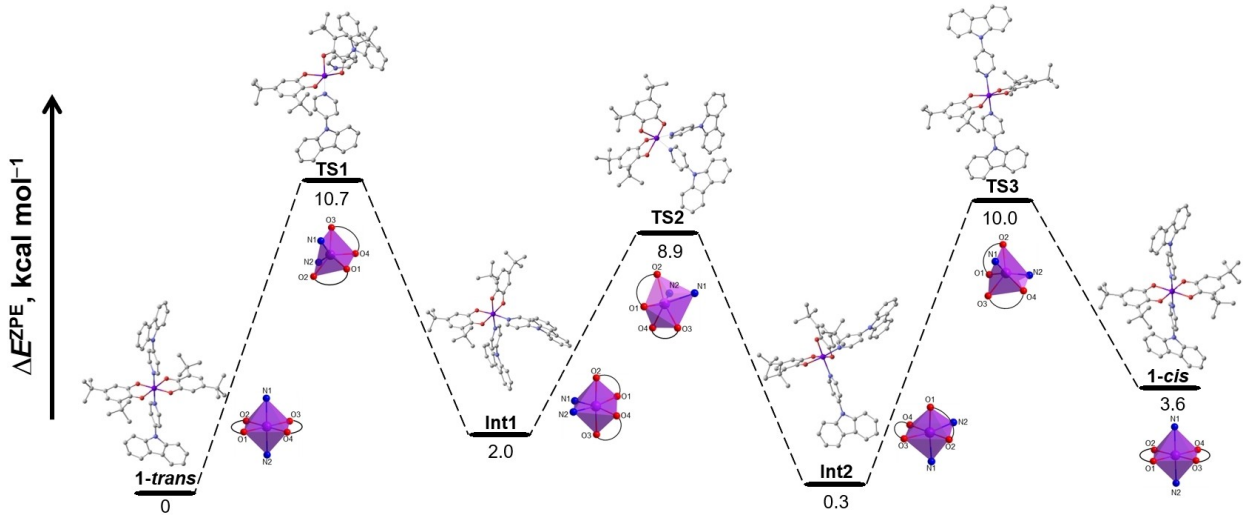

Figure 5. Energy profile and optimized geometries of structures on the pathway of the isomerization transformation process of **1-*trans*** (HS-Co^{II}–$Sq^{\bullet-}$/$Sq^{\bullet-}$) into **1-*cis*** (HS-Co^{II}–$Sq^{\bullet-}$/$Sq^{\bullet-}$) involving concerted bond rotation, calculated by the DFT UTPSSh/6-311++G(d,p) method.

ments occur via ***TS2*** ($\Delta E^{ZPE} = 8.9\,kcal\,mol^{-1}$). Gradient descent along the transition vector from ***TS2*** in the direction of the reaction products results in the formation of ***Int2*** ($\Delta E^{ZPE} = 0.3\,kcal\,mol^{-1}$), the geometry characteristics of which are close to those found for ***Int1***. At the final stage, the system converts into the **1-*cis*** via transition state ***TS3***. The energy barriers that need to be overcome for realization of the proposed mechanism do not exceed 11 $kcal\,mol^{-1}$, which points to thermal accessibility of this reaction pathway.

The feasibility of an intramolecular bond-rupture mechanism was also evaluated through calculations. The results suggest that if *trans*-to-*cis* isomerization involves Co–O/Co–N bond breakage (Figure S24–26 and Table S9,10), the process requires overcoming an energy barrier of nearly 20 $kcal\,mol^{-1}$. This is substantially higher than the energy barrier associated with the previously discussed twist mechanism. Therefore, it is evident that the bond-rupture twist mechanism is less energetically favorable than the non-bond-rupture twist mechanism. It is important to note, however, that without additional experimental or exhaustive computational endeavors—beyond the scope of this study—bond-rupture mechanisms cannot be definitively ruled out.

Conclusion

We have uncovered a thermal-activated molecular twist-induced isomerization from **1-*trans*** to **1-*cis*** in the solid state that triggers a pronounced two-step VT transition. In-depth analysis including *in situ* SCSC studies, DSC measurements, and DFT calculations have elucidated the underlying mechanism involving structural rearrangement that potentially occurs through a non-bond-rupture twist mechanism, which demonstrating the critical role of a synchronized crystal melting-recrystallization phase transition process accompanying the VT transition. The use of the sterically hindered monodentate ligand (pycz) provides great spatial freedom and reaction cavity, which facilitates the isomerization process in a closely packed structure. Additionally, it potentially acts as a template for efficient recrystallization. Furthermore, twist mechanisms such as the renowned Bailar and Rây–Dutt twists are predominantly observed in solution. The potential observation of such mechanisms in the solid state represents a significant contribution, filling a notable knowledge gap in textbooks and the existing literature. This unprecedented behavior highlights the potential of isomerization-induced structural transformation as a powerful tool for tailoring the properties of VT complexes. The intricate relationship between molecular structure and activity uncovered in this work has broader implications for the development of switchable molecule-based materials for a wide range of applications.

Supporting Information

Experimental section, additional measurements, theoretical calculations, additional Figures and tables (PDF). Video S1 for the crystal surface's melting-recrystallization (mp4). CCDC 2287997 (for **1-*trans*·*S***), 2287995 (for **1-*trans*** at 150 K), 2287996 (for **1-*trans*** at 340 K), 2287993 (for **1-*cis*** at 150 K), 2287998 (for **1-*cis*** at 270 K), 2287994 (for **1-*trans*** at 365 K).[24]

Acknowledgements

This work was supported by the National Natural Science Foundation of China (Grants 22371015 and 22101021). We thank the Chemistry and Chemical Experiment Center and the Analysis & Testing Center of Beijing Institute of Technology for technique supports. A.A.S. and M.G.C. acknowledge the financial support from Ministry of Science

and Higher Education of the Russian Federation (State assignment in the field of scientific activity, project No. FENW-2023-0017) for computational studies. A.A.G. acknowledges financial support from Ministry of Science and Higher Education of the Russian Federation (Agreement 075-15-2021-1363) for the in situ XAS measurements.

Conflict of Interest

The authors declare no conflict of interest.

Data Availability Statement

The data that support the findings of this study are available in the supplementary material of this article.

Keywords: Valence Tautomerism · Molecular Twist · Magnetic Properties · SCSC Transformation · DFT Calculation

[1] a) T. Tezgerevska, K. G. Alley, C. Boskovic, *Coord. Chem. Rev.* **2014**, *268*, 22–40; b) O. Sato, J. Tao, Y.-Z. Zhang, *Angew. Chem. Int. Ed.* **2007**, *46*, 2152–2187; *Angew. Chem.* **2007**, *119*, 2200–2236; c) M. Wang, Z.-Y. Li, R. Ishikawa, M. Yamashita, *Coord. Chem. Rev.* **2021**, *435*, 213819.

[2] a) J. Tao, H. Maruyama, O. Sato, *J. Am. Chem. Soc.* **2006**, *128*, 1790–1791; b) P. Dapporto, A. Dei, G. Poneti, L. Sorace, *Chem. Eur. J.* **2008**, *14*, 10915–10918; c) O. Drath, R. W. Gable, B. Moubaraki, K. S. Murray, G. Poneti, L. Sorace, C. Boskovic, *Inorg. Chem.* **2016**, *55*, 4141–4151; d) G. K. Gransbury, B. N. Livesay, J. T. Janetzki, M. A. Hay, R. W. Gable, M. P. Shores, A. Starikova, C. Boskovic, *J. Am. Chem. Soc.* **2020**, *142*, 10692–10704; e) J.-P. Wang, W.-T. Liu, M. Yu, X.-Y. Ji, J.-L. Liu, M.-Z. Chi, A. A. Starikova, J. Tao, *Inorg. Chem.* **2022**, *61*, 4428–4441.

[3] a) A. Witt, F. W. Heinemann, M. M. Khusniyarov, *Chem. Sci.* **2015**, *6*, 4599–4609; b) M. M. Paquette, D. Plaul, A. Kurimoto, B. O. Patrick, N. L. Frank, *J. Am. Chem. Soc.* **2018**, *140*, 14990–15000; c) J.-W. Dai, Y.-Q. Li, Z.-Y. Li, H.-T. Zhang, C. Herrmann, S. Kumagai, M. Damjanović, M. Enders, H. Nojiri, M. Morimoto, N. Hoshino, T. Akutagawa, M. Yamashita, *Natl. Sci. Rev.* **2023**, *10*, nwad047.

[4] A. Panja, N. C. Jana, A. Bauzá, A. Frontera, C. Mathonière, *Inorg. Chem.* **2016**, *55*, 8331–8340.

[5] a) K. G. Alley, G. Poneti, P. S. D. Robinson, A. Nafady, B. Moubaraki, J. B. Aitken, S. C. Drew, C. Ritchie, B. F. Abrahams, R. K. Hocking, K. S. Murray, A. M. Bond, H. H. Harris, L. Sorace, C. Boskovic, *J. Am. Chem. Soc.* **2013**, *135*, 8304–8323; b) R. D. Schmidt, D. A. Shultz, J. D. Martin, *Inorg. Chem.* **2010**, *49*, 3162–3168; c) R. D. Schmidt, D. A. Shultz, J. D. Martin, P. D. Boyle, *J. Am. Chem. Soc.* **2010**, *132*, 6261–6273.

[6] a) G. K. Gransbury, M.-E. Boulon, S. Petrie, R. W. Gable, R. J. Mulder, L. Sorace, R. Stranger, C. Boskovic, *Inorg. Chem.* **2019**, *58*, 4230–4243; b) Y.-M. Zhao, J.-P. Wang, X.-Y. Chen, M. Yu, A. A. Starikova, J. Tao, *Inorg. Chem. Front.* **2023**, *10*, 7251–7264.

[7] a) X.-Y. Chen, R.-J. Wei, L.-S. Zheng, J. Tao, *Inorg. Chem.* **2014**, *53*, 13212–13219; b) Y. Mulyana, G. Poneti, B. Moubaraki, K. S. Murray, B. F. Abrahams, L. Sorace, C. Boskovic, *Dalton Trans.* **2010**, *39*, 4757–4767.

[8] P. Wang, S. Yergeshbayeva, X. Lin, S. Bisht, M. Gakiya-Teruya, M. Shatruk, *Cryst. Growth Des.* **2023**, *23*, 2384–2394.

[9] K. Kc, T. Woods, L. Olshansky, *Angew. Chem. Int. Ed.* **2023**, *62*, e202311790; *Angew. Chem.* **2023**, *135*, e202311790.

[10] a) R. M. Wood, G. J. Palenik, *Inorg. Chem.* **1998**, *37*, 4149–4151; b) O. Carugo, C. B. Castellani, K. Djinović, M. Rizzi, *J. Chem. Soc. Dalton Trans.* **1992**, 837–841; c) S. N. Brown, *Inorg. Chem.* **2012**, *51*, 1251–1260.

[11] O.-S. Jung, C. G. Pierpont, *J. Am. Chem. Soc.* **1994**, *116*, 2229–2230.

[12] a) C. Lefebvre, G. Rubez, H. Khartabil, J.-C. Boisson, J. Contreras-García, E. Hénon, *Phys. Chem. Chem. Phys.* **2017**, *19*, 17928–17936; b) T. Lu, Q. Chen, *J. Comput. Chem.* **2022**, *43*, 539–555.

[13] M. E. Brown, A. K. Galwey, *Thermochim. Acta* **1979**, *29*, 129–146.

[14] P. O'Brien, *Polyhedron* **1983**, *2*, 233–243.

[15] R. S. Bogadi, D. C. Levendis, N. J. Coville, *J. Am. Chem. Soc.* **2002**, *124*, 1104–1110.

[16] a) M. D. Bala, N. J. Coville, *J. Organomet. Chem.* **2007**, *692*, 709–730; b) L. Cheng, N. J. Coville, *Thermochim. Acta* **1998**, *319*, 27–32.

[17] M. Seredyuk, A. B. Gaspar, V. Ksenofontov, Y. Galyametdinov, J. Kusz, P. Gütlich, *Adv. Funct. Mater.* **2008**, *18*, 2089–2101.

[18] D. N. Hendrickson, C. G. Pierpont, *Top. Curr. Chem.* **2004**, *234*, 63–95.

[19] a) N. Serpone, D. G. Bickley, *Prog. Inorg. Chem.* **1972**, *17*, 391–566; b) H. S. Rzepa, M. E. Cass, *Inorg. Chem.* **2007**, *46*, 10444–10444; c) M. Amati, F. Lelj, *Theor. Chem. Acc.* **2008**, *120*, 447–457.

[20] a) F. Riblet, G. Novitchi, R. Scopelliti, L. Helm, A. Gulea, A. E. Merbach, *Inorg. Chem.* **2010**, *49*, 4194–4211; b) A. V. Davis, T. K. Firman, B. P. Hay, K. N. Raymond, *J. Am. Chem. Soc.* **2006**, *128*, 9484–9496.

[21] D. L. Kepert, *Prog. Inorg. Chem.* **1977**, *23*, 1–65.

[22] a) A. Gavriluta, G. E. Büchel, L. Freitag, G. Novitchi, J. B. Tommasino, E. Jeanneau, P.-S. Kuhn, L. González, V. B. Arion, D. Luneau, *Inorg. Chem.* **2013**, *52*, 6260–6272; b) S. Bhattacharya, S. R. Boone, G. A. Fox, C. G. Pierpont, *J. Am. Chem. Soc.* **1990**, *112*, 1088–1096.

[23] a) A. Dei, A. Feis, G. Poneti, L. Sorace, *Inorg. Chim. Acta* **2008**, *361*, 3842–3846; b) A. Dei, L. Sorace, *Appl. Magn. Reson.* **2010**, *38*, 139–153; c) M. P. Bubnov, N. A. Skorodumova, A. S. Bogomyakov, G. V. Romanenko, A. V. Arapova, K. A. Kozhanov, N. N. Smirnova, G. A. Abakumov, V. K. Cherkasov, *Russ. Chem. Bull.* **2011**, *60*, 449–455.

[24] Deposition numbers 2287997 (for **1-*trans-S***), 2287995 (for **1-*trans*** at 150 K), 2287996 (for **1-*trans*** at 340 K), 2287993 (for **1-*cis*** at 150 K), 2287998 (for **1-*cis*** at 270 K), 2287994 (for **1-*trans*** at 365 K) contain the supplementary crystallographic data for this paper. These data are provided free of charge by the joint Cambridge Crystallographic Data Centre and Fachinformationszentrum Karlsruhe Access Structures service.

Manuscript received: January 28, 2024
Accepted manuscript online: March 7, 2024
Version of record online: March 25, 2024